

1 **Interpreting the $^{13}\text{C}/^{12}\text{C}$ ratio of carbon dioxide in an urban airshed in the Yangtze**
2 **River Delta, China**

3
4 Jiaping_Xu¹, Xuhui Lee^{1,2*}, Wei Xiao¹, Chang Cao¹, Shoudong Liu¹, Xuefa Wen³, Jingzheng
5 Xu¹, Zhen Zhang¹, Jiayu Zhao¹

6
7 ¹Yale-NUIST Center on Atmospheric Environment, Nanjing University of Information
8 Science & Technology, Nanjing, China

9
10 ²School of Forestry and Environmental Studies, Yale University, New Haven, Connecticut,
11 USA

12
13 ³Key Laboratory of Ecosystem Network Observation and Modeling, Institute of Geographic
14 Sciences and Natural Resources Research, Chinese Academy of Sciences, Beijing, China

15
16 * Corresponding author

17 Dr. Xuhui Lee

18 Sara Shallenberger Brown Professor

19 School of Forestry and Environmental Studies, Yale University,

20 21 Sachem Street, New Haven, Connecticut 06510, USA

21 Phone: (203)432-6271; Fax: (203)432-5023

22 E-mail: xuhui.lee@yale.edu

23

24 **Abstract:** Observations of atmospheric CO₂ mole fraction and the ¹³C/¹²C ratio (expressed as
25 δ¹³C) in urban airsheds provide constraints on the roles of anthropogenic and natural sources
26 and sinks in local and regional carbon cycles. In this study, we report observations of these
27 quantities in Nanjing at hourly intervals from March 2013 to August 2015 using a laser-based
28 optical instrument. Nanjing is the second largest city located in the highly industrialized
29 Yangtze River Delta (YRD), Eastern China. The mean CO₂ mole fraction and δ¹³C were
30 (439.7 ± 7.5) μmol mol⁻¹ and (-8.48 ± 0.56) ‰ over this observational period. The peak
31 monthly mean δ¹³C (-7.44 ‰, July 2013) was 0.74 ‰ higher than that observed at Mount
32 Waliguan, a WMO baseline site on the Tibetan Plateau and upwind of the YRD region. The
33 highly ¹³C-enriched signal was partly attributed to the influence of cement production in the
34 region. By applying the Miller-Tans method to nighttime and daytime observations to
35 represent signals from the city of Nanjing and the YRD, respectively, we showed that the
36 ¹³C/¹²C ratio of CO₂ sources in the Nanjing Municipality was (0.21 ± 0.53) ‰ lower than that
37 in the YRD. Flux partitioning calculations revealed that natural ecosystems in the YRD were
38 a negligibly small source of atmospheric CO₂.

39

40 **Keywords:** urban areas; CO₂ flux; Industrial process; Carbon isotope; In-situ observation

41

42 **1 Introduction**

43 Atmospheric CO₂ sources and sinks in urban areas consist mainly of plant uptake and release
44 and fossil fuel combustion. These contributors have unique ¹³C/¹²C ratios. City clusters are
45 human-dominated systems with high carbon emission intensity, contributing over 70% of the
46 total anthropogenic CO₂ to the atmosphere (Satterthwaite 2008). Previous urban isotopic
47 studies emphasize carbon emissions from fossil combustion (Zondervan and Meijer 1996,
48 Pataki et al. 2003, Zimnoch et al. 2004, Affek and Eiler 2006, Newman et al. 2008).
49 Relatively little attention is given to the $\delta^{13}\text{C}$ of carbon dioxide released by cement
50 production, which is much higher than that of fossil fuel origin (Andres et al. 1994).
51 Likewise, the CO₂ emitted from burning of minerals in non-energy consumption industrial
52 processes, such as iron and steel production, has higher $\delta^{13}\text{C}$ than that of fossil fuel (Table 2,
53 Widory 2006). In China, cement production and industrial processes contribute 13 % of the
54 total anthropogenic CO₂ emission (Mu et al. 2013). Many of these industrial activities occur
55 in or near urban areas. So far, little is known about their roles in the atmospheric carbon
56 stable isotope budget.

57 One scientific motivation for quantifying the $\delta^{13}\text{C}$ of atmospheric CO₂ is that it provides
58 constraints that allow partitioning of the net surface flux into component fluxes (Farquhar and
59 Lloyd 1993, Yakir and Sternberg 2000, Pataki et al. 2003). The ¹³C-based partitioning method
60 has been used primarily for vegetation ecosystems, such as forests (Lloyd et al. 1996, Lloyd
61 et al. 2001, Ometto, et al. 2006, Zobitz et al. 2008), grasses (Ometto et al. 2002, Pataki et al.
62 2003), and crops (Leavitt et al. 1995, Griffis et al. 2005). The approach has also been used in
63 a limited number of urban studies (Pataki et al. 2003, Zimnoch et al. 2004, Newman et al.

64 2008, Jasek et al. 2014). Compared with vegetation ecosystems, urban ecosystems have more
65 complex CO₂ source configurations. We must consider both natural sources (plants and soils)
66 and anthropogenic sources (fossil combustion and non-energy industrial processes) and the
67 fact that the degree of mixing of urban air with the free troposphere and the air outside the
68 urban boundary varies diurnally and seasonally. Anthropogenic emissions are hard to quantify
69 because they depend on multiple factors including city size, population density, fossil mix,
70 and climate.

71 One of the first measurements of the carbon isotope ratio of CO₂ in an urban atmosphere
72 was made by Friedman and Irsa (1967). Since then, more experiments have been conducted
73 in urban environments (Ehleringer et al. 2002, Koerner and Klopatek 2002, Takahashi et al.
74 2002, Clark-Thorne and Yapp 2003, Lichtfouse et al. 2003, Widory and Javoy 2003, Zimnoch
75 et al. 2004, Bush et al. 2007, Guha and Ghosh 2010, Wang and Pataki 2012). The analytical
76 technique employed in these studies is mainly based on isotope-ratio mass-spectrometry
77 (IRMS). In recent years, the development of isotope ratio infrared spectroscopy (IRIS) and
78 on-line calibration technology provides a new solution for long-term in-situ observation of
79 the CO₂ mole fraction and $\delta^{13}\text{C}$ at high frequencies (1 Hz to 1 hour; Pataki et al. 2006, Griffis.
80 2013, Gorski et al. 2015). However, application of the IRIS technology in urban monitoring
81 is still limited in terms of cities covered and measurement duration (McManus et al. 2002,
82 Pataki et al. 2006, Wada et al. 2011, Moore and Jacobson (2015). Only a few published
83 studies have presented data that span one full annual cycle (e.g., Pang et al. 2016).

84 Simultaneous measurement of atmospheric CO₂ concentration and $\delta^{13}\text{C}$ is used to
85 determine the overall $^{13}\text{C}/^{12}\text{C}$ ratio of local surface sources δ_s . The majority of published

86 urban studies to date have deployed the Keeling plot method (Keeling 1958, Keeling 1961)
87 for the determination of δ_s . In this approach, a linear relationship is established between $\delta^{13}\text{C}$
88 and the reciprocal of the CO_2 mole fraction from the observed time series, and the intercept
89 of the linear regression is taken as the isotopic ratio of the local CO_2 emissions. The method
90 assumes that the isotopic ratio of the sources is invariant with time. It also assumes that
91 changes in the CO_2 mole fraction and in $\delta^{13}\text{C}$ are attributed only to the surface sources and
92 are unaffected by regional carbon sources (Pataki et al. 2003). However, these assumptions
93 do not strictly hold in an urban environment because the intensity of traffic emissions varies
94 strongly through the diel cycle (McDonald et al. 2014), and therefore the composition of the
95 surface source varies, and its $^{13}\text{C}/^{12}\text{C}$ ratio cannot be assumed constant. In addition, because
96 of strong atmospheric mixing in the daytime convective boundary layer, the background air
97 in the upper troposphere can be easily entrained to the surface layer, mixing the CO_2 that
98 originates from regional sources with that emitted locally in the urban airshed.

99 Miller and Tans (2003) propose that δ_s be determined as the slope of the linear
100 relationship

$$101 \quad \delta_a C_a - \delta_b C_b = \delta_s (C_a - C_b) \quad (1)$$

102 where C_a is CO_2 mole fraction in urban air, C_b is CO_2 mole fraction at a background site, δ_a is
103 the $\delta^{13}\text{C}$ value of C_a , and δ_b is the $\delta^{13}\text{C}$ value of C_b . All the variables are time dependent.

104 Because this approach takes into account the fact the background atmosphere varies, it may
105 be more suitable than the Keeling method for inferring δ_s from the observations made in the
106 urban area with complex emission sources. The method has been applied to local and
107 regional carbon budget studies in nonurban settings (Miller et al. 2003) and in an urban

108 environment by Newman et al. (2016). Here we extend the method to continuous
109 measurements in an urban environment.

110 In this study, we report the results of long-term (30 months) continuous measurement of
111 atmospheric CO₂ mole fraction and $\delta^{13}\text{C}$ at a suburban site in Nanjing using an IRIS
112 instrument. Nanjing is the second largest city in the Yangtze River Delta (YRD), Eastern
113 China, with a built-up area of 753 km² and a population of 8.2 million. Geographically, the
114 YRD includes the provinces of Jiangsu, Zhejiang and Anhui and the Shanghai municipality
115 (29.04° to 33.41° N, 118.33° to 122.95° E) with a population of 190 million. The YRD is
116 influenced by subtropical moist monsoon climate. The mean annual temperature is about 15
117 °C and the annual precipitation is between 1000 mm and 1800 mm. The vegetation types are
118 all C3 species. The YRD is the most industrialized region in China and had a higher urban
119 land fraction of 10.8 % as of 2014 than the global mean (2.4 %, Akbari et al. 2009). In 2014,
120 more than 220 large cement production factories (daily output exceeding 1000 tons) were
121 located in the YRD (China Cement, 2016), contributing about 20 % of the national cement
122 output.

123 The objectives of this study are (1) to characterize the atmospheric $\delta^{13}\text{C}$ diel, seasonal and
124 annual variations in this urban environment, in a region where such measurement is
125 nonexistent, (2) to investigate the influence of cement production on atmospheric $\delta^{13}\text{C}$, (3) to
126 evaluate the performance of the Keeling plot and the Miller-Tans methods for determining δ_s ,
127 and (4) to explore the utility of the isotopic constraints for inferring the net surface flux and
128 the plant CO₂ flux in Nanjing and in the YRD.

129

130 **2 Methods**

131 **2.1 Atmospheric observation**

132 An IRIS analyzer (model G1101-i, Picarro Inc., Sunnyvale, CA) was used to measure
133 atmospheric CO₂ mole fraction and ¹³C/¹²C ratio ($\delta^{13}\text{C}$) continuously from February 2013 to
134 August 2015. The analyzer was housed on the 9th floor of our laboratory building on the
135 campus of Nanjing University of Information, Science and Technology (NUIST, 32°12' N,
136 118°43' E), in the northern suburb of Nanjing, at a linear distance of 20 km to the city center.
137 The instrument inlet was at a height of 34 m above the ground. There was no large industrial
138 CO₂ source in the 3 km radius except for a commuting road located about 300 m east of the
139 observation site. The nearest industrial complex, the Nanjing Iron & Steel Group Co. Ltd. and
140 the Nanjing Chemical Industry Group, was located about 5 km to the south of the site.

141 The measurement was made at 0.3 Hz and at an air flow rate of 30 mL min⁻¹ at standard
142 temperature and pressure. One three-way solenoid valve was combined with two two-way
143 solenoid valves, so the analyzer could be switched for atmospheric sampling and for
144 sampling of two standard gases. Calibration was carried out every 3 h by sampling each
145 standard gas for 5 minutes following the procedure of Bowling et al. (2003) and Wen et al.
146 (2013). [To avoid transient effects, only the data collected in the last 2 minutes of the 5-min
147 calibration periods was used (Supplementary Figure S1).] Table 1 lists the concentrations and
148 their isotopic ratios of the standard gases used in this study. These gases were balanced in air,
149 and their concentration values bracketed the range of ambient concentration variability
150 (Figure 3 below). Their CO₂ mole fractions were measured with a gas analyzer (model
151 (model G1301, Picarro) and calibrated against three primary standards obtained from NOAA-

152 ESRL which were traceable to the WMO 2007 scale reported by the Central Calibration
153 Laboratory of the World Meteorological Organization, and their $\delta^{13}\text{C}$ values were measured
154 with a mass spectrometer (MAT-253, Finnigan) using IAEA reference materials IAEA-CO-8
155 (-5.76 ‰ VPDB) and IAEA-CO-9 (-47.32 ‰ VPDB). The mass spectrometer measurements
156 of these reference materials were (-5.81 ± 0.04) ‰ and (-46.64 ± 0.08) ‰. The ambient
157 measurement was averaged to hourly intervals. The isotopic ratio was expressed in the delta
158 notation ($\delta^{13}\text{C}$) in reference to the VPDB scale.

159 The typical 5-min measurement precision is 0.3 ‰ for $\delta^{13}\text{C}$ and 0.05 $\mu\text{mol mol}^{-1}$ for
160 CO_2 mole fraction according to the instrument manufacturer. Our own Allan variance
161 analysis revealed a precision of 0.05 ‰ for $\delta^{13}\text{C}$ and 0.07 $\mu\text{mol mol}^{-1}$ for CO_2 mole fraction at
162 the hourly averaging interval. These improvements were simply statistical, due to the increase
163 in the number of samples being used for averaging. The precision of the ambient
164 measurement was lower than this due to errors propagated through the calibration procedure.
165 According to a laboratory test on an analyzer of the same model and using the same
166 calibration procedure as ours, the hourly $\delta^{13}\text{C}$ precision is about 0.4 ‰ (Wen et al., 2013).

167 The calibration gases had much lower $\delta^{13}\text{C}$ than the ambient delta values. The mismatch
168 in the delta value between the calibration standard and the ambient air is common in
169 applications of the IRIS technique [$^{13}\text{C}(\text{CH}_4)$, Röckmann et al. 2016; $^{18}\text{O}(\text{H}_2\text{O})$, Lee et al.
170 2005; $^{13}\text{C}(\text{CO}_2)$, Bowling et al. 2003]. For example, Bowling et al. (2003) used calibration
171 standards with delta values of -29.55 ‰ and -40.58 ‰ to calibrate their optical $^{13}\text{C}(\text{CO}_2)$
172 instrument. But because the system measures the concentrations of the major and the minor
173 isotopologue independently, it is not critical that the calibration standards and the

174 measurement target have matching isotope ratios, so long as the standards bracket
175 concentration variability of the target (Bowling et al. 2005). Nevertheless, the overall
176 accuracy of the measurement may be further improved by using calibration standards that
177 bracket variations in both the concentration and the delta values of ambient air samples. We
178 could not implement this improved calibration procedure because our analyzer failed at the
179 end of the experiment.

180 We did not adopt the strict filtering technique used for background sites (Thoning et al.
181 1989) because of high natural variations in urban airsheds. We removed the first 3 min of the
182 data after switching to the ambient sampling mode from the calibration mode. Additionally,
183 data were removed if the average hourly CO₂ mole fraction was lower than 390 μmol mol⁻¹
184 (or 30 μmol mol⁻¹ lower than the midafternoon value in the summer; Figure 3 below) or δ¹³C
185 were out of the range between -15 ‰ and -5.5 ‰ (or about 3 standard deviations from the
186 mean); A total of 217 hourly values were removed by these outlier criteria.

187 The δ¹³C value measured by the analyzer in high humidity conditions is biased high due
188 to spectral broadening and direct spectral interference (Rella 2011). To correct for the
189 humidity interference, we carried out two tests using a dew-point generator (model 610, LI-
190 COR, Inc., Lincoln, NE). A CO₂ standard gas (secondary standard gas, 439 μmol mol⁻¹ in test
191 one and 488 μmol mol⁻¹ in test two, balanced by dry air) was fed into the dew-point
192 generator. The outlet of the dew-point generator was connected with a 3-way union with one
193 end linked to the inlet of the analyzer and the other open to the room. The humidity level of
194 the air coming out of the dew point generator was regulated at eight levels in a dew-point
195 temperature range of 1 to 30 °C, giving a water vapor mole fraction ranging from 0.66 % to

196 4.26 % (0.66 to 4.26 cmol mol⁻¹). Measurement at each humidity level lasted 30 min, with the
 197 first 5 min excluded from the analysis. Because the ¹³C/¹²C ratio of the standard gas was
 198 constant, any observed variations were caused by the humidity artifact. We found that no
 199 correction was needed for our analyzer if the water vapor mole fraction was below 2.03 %.
 200 Above this humidity level, the measurement was biased high by 0.46 ‰ for every 1 cmol
 201 mol⁻¹ increase in the water vapor mole fraction (Figure 1). This humidity effect is not
 202 negligible, but is an order of magnitude smaller than that reported by Rella (2011). The two
 203 tests, taken eight months apart, yielded essentially the same result. The correction equation is

$$204 \quad \delta^{13}\text{C} = \delta^{13}\text{C}_{\text{true}} \quad \text{C}(\text{H}_2\text{O}) \leq 2.03 \text{ \%} \quad (2a)$$

$$205 \quad \delta^{13}\text{C} = \delta^{13}\text{C}_{\text{true}} + 0.46 \text{ ‰} (\text{C}(\text{H}_2\text{O}) \text{ \%} - 2.03 \text{ \%}) \quad \text{C}(\text{H}_2\text{O}) > 2.03 \text{ \%} \quad (2b)$$

206 where C(H₂O) is water vapor mole fraction and was measured by the same isotope analyzer,
 207 $\delta^{13}\text{C}$ is the measured isotope delta value (after the two-point calibration), and $\delta^{13}\text{C}_{\text{true}}$ is the
 208 true isotope delta value. The ambient vapor mole fraction varied from 0.16 to 3.64 % during
 209 the measurement period. About 35 % of the observations exceeded the threshold mole
 210 fraction of 2.03 % and required correction. The largest hourly correction was 0.74 ‰. In the
 211 following, all the data have been corrected for the humidity interference.

212

213 **2.2 The ¹³C/¹²C ratio of surface sources (δ_s)**

214 We applied the Miller-Tans method to estimate the ¹³C/¹²C ratio of the surface source (δ_s).
 215 Strictly, Equation 1 does not allow a non-zero intercept. When applied to the urban airshed in
 216 Los Angeles, Equation 1 does not require an intercept (Newman et al. 2016). But when applied
 217 to the data obtained at the monthly time scale in this study, the regression yielded a non-zero

218 intercept (Supplementary Figure S2). To determine if a shorter time scale would improve the
219 result, we applied the 5-h moving window technique described by Vardag et al. (2016) to the
220 observations made in January and July 2014. Only 4 % of the data, all obtained at nighttime,
221 satisfies their data screening criteria. The mean regression equation of this subset is $y = (-$
222 $26.41 \pm 4.03) x + (428.84 \pm 211.12)$ for January and $y = (-25.64 \pm 6.39) x + (687.83 \pm 264.67)$
223 for July, where x is $(C_a - C_b)$ and y is $(\delta_a C_a - \delta_b C_b)$. In these analyses, the background CO₂
224 mole fraction and the isotope ratio were those observed at Mount Waliguan (WLG, 36°17' N,
225 100°54' E, 3816 m above the mean sea level;
226 <https://www.esrl.noaa.gov/gmd/dv/data/index.php>) located at the northeastern edge of the
227 Tibetan Plateau (Zhou et al., 2005), the closest upwind WMO background station for
228 Nanjing. Use of other WMO baseline sites as the background gave essentially the same
229 results.

230 The selection of a background site is a critical issue when applying the Miller-Tans
231 method (Ballantyne et al., 2011 & 2010). That the Miller-Tans intercept does not go to zero
232 suggests that the baseline site WLG may not be a suitable background for this highly
233 urbanized region. We tested the Miller-Tans method with other isotope data published for
234 urban areas, and found that the intercept was nonzero for the data obtained by Sturm et al.
235 (2006) at Bern, Switzerland (Supplementary Figure S3) and a number of other urban datasets
236 (Supplementary Table S1).

237 In the following, we used the tropospheric CO₂ mole ratio calculated by CarbonTracker
238 over the YRD region (altitude 3330 m; <https://www.esrl.noaa.gov/gmd/dv/data/index.php>) as
239 the background concentration (C_b). The CarbonTracker mole ratio is on average 3.5 μmol

240 mol⁻¹ higher than that observed at WLG. To overcome the problem that CarbonTracker does
241 not calculate tropospheric $\delta^{13}\text{C}$, we rearranged Equation 1 to a form that allows an intercept
242 but without the need for a known background $\delta^{13}\text{C}$, as

$$243 \quad \delta_a C_a = \delta_s (C_a - C_b) + \delta_b C_b \quad (3)$$

244 The $^{13}\text{C}/^{12}\text{C}$ ratio of the surface source was taken as the slope of the linear regression of $\delta_a C_a$
245 against $(C_a - C_b)$. A key difference between Equation 3 here and Equation 5 of Miller and Tans
246 (2003) is that the δ_s appears only in the slope parameter in Equation 3 but in both the slope
247 and the intercept parameter in Miller and Tans' Equation 5. This modified Miller-Tans
248 analysis requires knowledge of background CO_2 mole fraction but not δ_b .

249 The Miller-Tans analysis was performed over monthly intervals, using the data collected
250 in daytime hours (10:00 to 16:00 local time) to represent YRD and data collected during
251 nighttime hours (22:00-6:00 local time) to represent Nanjing. Morning and evening
252 transitional periods were omitted to avoid the confounding effects of sign change of the
253 biological CO_2 flux and sudden changes in the atmospheric stability regime.

254 We interpreted the daytime results to represent the influence of surface sources in the
255 YRD region and the nighttime results to represent the influence of surface sources in the
256 Nanjing municipality. The vigorous turbulent exchange in the daytime boundary layer
257 diminishes the role of local sources in the measured concentration and isotopic ratio. In other
258 words, the daytime measurement has a much larger source footprint than the size of the urban
259 land itself or the footprint of the nighttime measurement. In contrast, the buildup of CO_2 at
260 night is primarily the result of sources in the city (Shen et al. 2014), so we considered the δ_s
261 determined from the nighttime observations to represent the signal of the sources located in

262 the city. Admittedly, this interpretation of daytime versus nighttime source areas is a
263 simplification because the actual source area also depends on thermal stratification and
264 boundary layer wind. Nevertheless, it is supported by a trajectory analysis and by an analysis
265 of the atmospheric methane to CO₂ emissions ratio (Shen et al. 2014).

266 For the purpose of comparing with the Miller-Tans results, we also estimated the source
267 ¹³C/¹²C ratio using the Keeling mixing line method. According to Wehr and Saleska (2017),
268 for the measurement uncertainties of our instrument system, the ordinary least squares
269 procedure has much lower bias errors of parameter estimation than the geometric mean
270 regression. In the following, the results of both the Miller-Tans method and the Keeling
271 mixing line method were based on the ordinary least squares regression.

272

273 **2.3 Inventory of anthropogenic sources**

274 We calculated the anthropogenic CO₂ fluxes from energy consumption and industrial process
275 following the SCOPE 1 procedure issued by the International Council for Local
276 Environmental Initiatives (ICLEI, 2008). The procedure considers only emissions from
277 sources that lie within the geographic boundary of investigation. The energy consumption
278 source consists of direct emissions from the three main energy consumption sectors (industry,
279 transport, and household). We ignored the commerce sector here because the main energy
280 consumption in this sector in Nanjing and in the YRD was electric power generated by coal
281 and coal consumption which was already considered in SCOPE 1. The amounts of CO₂
282 emission were estimated with the IPCC methodology adopting the emission factors for each
283 fossil fuel type recommended by IPCC. The calculations were done separately for the YRD

284 region and for the Nanjing municipality. Because no statistical data were available for energy
285 consumption in the transport sector in Nanjing, the CO₂ emission from the transport sector
286 was deduced according to vehicle number, average annual driving distance and coefficients
287 of fuel economy (Bi et al. 2011). We obtained the data on energy consumption from official
288 sources (CESY 2013, CSY 2013, NSY, 2013).

289 The non-energy industrial processes included cement, raw iron, crude steel, and
290 ammonia synthesis processes. In the YRD, the data were available at monthly intervals. For
291 the city of Nanjing, only annual statistics were available.

292

293 **2.4 Partitioning the net surface flux**

294 We partitioned the surface CO₂ flux (F_S) into three component fluxes according to the
295 following mass conservation equations

$$296 \quad F_S = F_F + F_C + F_P \quad (4)$$

$$297 \quad \delta_S F_S = \delta_F F_F + \delta_C F_C + \delta_P F_P \quad (5)$$

298 where F_F is the flux from fossil fuel combustion and industrial emission except cement
299 production (termed “fossil plus”), F_C is the flux due to cement production, F_P is the biological
300 flux, and δ_F, δ_C, and δ_P are the δ¹³C value of F_F, F_C and F_P, respectively. These CO₂ mass
301 fluxes are obtained by dividing the total emission by the surface area within the geographic
302 boundary of Nanjing or the YRD, having dimensions of mg m⁻² s⁻¹. We separated the cement
303 source from other non-energy consumption industrial processes because its ¹³C/¹²C ratio is
304 much higher. In these equations, the monthly net surface flux (F_S) and the biological flux (F_P)
305 are unknowns to be solved for, and all other terms are either provided by the atmospheric

306 measurement or by the inventory calculation. The partitioning analysis was done for both
307 Nanjing and the YRD using the nighttime and daytime observations, respectively.

308 The value for δ_F was the weighted average of the isotope ratio of individual fuel types
309 and industrial processes (Table 2). The delta value of CO₂ from cement production is
310 provided by Anders (1994). We adopt a value of (-28.2 ‰) for δ_P for the YRD and Nanjing,
311 on account of a linear relationship between δ_P and tree age (Fessenden and Ehleringer 2002),
312 a typical tree age in this region (40 years) and a U-shaped relationship between δ_P and annual
313 precipitation (Pataki et al. 2007). Our δ_P is more negative than that reported for a boreal forest
314 (-26.2 ‰; Pataki et al. 2007) but is in closer agreement with the value reported for a Ginkgo
315 tree in Nanjing (-29.3 ‰; Sun et al. 2003). A summary of the isotopic ratios of the four
316 source categories is given in Table 3.

317 Uncertainties in the delta values of the different fuel types and industrial processes were
318 based on the data found in the references listed in Table 2. The uncertainty in δ_P was assumed
319 to be ± 1.00 ‰ (Verdag et al. 2016). The mass flux terms F_F and F_C were assumed to have a
320 10% uncertainty, which is typical of fossil fuel consumption data (Vardag et al. 2016).

321 To partition the nighttime flux for Nanjing, we assumed that the nighttime F_F was 20 %
322 of the daily value. The parameter 20 % was determined by the diel variation of the CO₂ flux
323 observed with an eddy covariance system in Nanjing (Bai 2011) and in several other cities
324 (Coutts et al. 2007, Song and Wang. 2011, Liu et al. 2012). At night, most of the factories in
325 the city were closed and the traffic flow was reduced to about 80 % of the daytime volume
326 (Yang et al. 2011).

327 The partitioning equations are explicit expressions of the mass balance principle. But
328 uncertainties in the isotope delta end members and the anthropogenic fluxes can propagate
329 through these equations, causing uncertainties in the estimation of F_S and F_P . Here we used a
330 Monte Carlo analysis to quantify the error propagation. The same analysis has been applied
331 to the partitioning of lake water budgets from isotope end members (Jasechko et al. 2014).
332 The procedure employed a Gaussian distribution for errors in the input variables and an
333 ensemble of 10,000 realizations for each month. Errors in F_S and F_P were computed as one
334 standard deviation of these realizations after excluding the top and bottom 50 extreme
335 ensemble members.

336

337 **3. Results**

338 **3.1. Temporal variations in the CO₂ mole fraction and $\delta^{13}\text{C}$**

339 The monthly CO₂ mole fraction during the summer was slightly lower than in the other
340 seasons (Figure 2). The mean mole fraction was 446.7 $\mu\text{mol mol}^{-1}$ and 431.1 $\mu\text{mol mol}^{-1}$ for
341 January and July, respectively, giving a seasonal amplitude of 15.6 $\mu\text{mol mol}^{-1}$. The mean
342 CO₂ mole fraction during the whole experimental period (March 2013 to August 2015) was
343 439.7 $\mu\text{mol mol}^{-1}$, which is 40.6 $\mu\text{mol mol}^{-1}$ higher than the value observed at WLG for the
344 same period. In 2014, the calendar year with complete data coverage, the mean CO₂ mole
345 fraction was 441.2 $\mu\text{mol mol}^{-1}$, which is 42.5 ppm higher than the WLG value for the same
346 year.

347 The $^{13}\text{C}/^{12}\text{C}$ ratio of atmospheric CO₂ displayed a more clear seasonal cycle than the
348 mole fraction (Figure 2). The monthly mean value was $(-9.07 \pm 0.17) \text{‰}$ (mean \pm standard

349 error) and $(-7.63 \pm 0.18) \text{‰}$ for January and July, respectively, with a seasonal amplitude of
350 1.44 ‰. The mean value for the whole experimental period was -8.48‰ , which is the same
351 as the WLG value (-8.48‰). The summertime (June to August) $\delta^{13}\text{C}$ was 0.39‰ higher than
352 the WLG background value. The seasonality of the $^{13}\text{C}/^{12}\text{C}$ ratio at Nanjing was greater than
353 that at WLG.

354 The strongest diel variation in the CO_2 mole fraction was observed in the autumn season
355 (September to November) and the weakest in the winter season (December to February), with
356 a diel amplitude of $27.9 \mu\text{mol mol}^{-1}$ and $13.4 \mu\text{mol mol}^{-1}$, respectively (Figure 3). In the
357 summer season, the peak value was observed at 07:00 and the lowest value at 19:00. In
358 contrast to the CO_2 mole fraction, $\delta^{13}\text{C}$ showed the lowest value in the early morning and the
359 highest value in the afternoon in all the four seasons. The diel amplitude was 1.36‰ in the
360 summer and 0.66‰ in the winter.

361

362 **3.2 $^{13}\text{C}/^{12}\text{C}$ ratio of the surface sources (δ_s)**

363 Figures 4 and 5 show an example of the modified Miller-Tans approach applied to the month
364 of January 2014. According to the slope parameter estimation, the $^{13}\text{C}/^{12}\text{C}$ ratio of the surface
365 sources was $(-25.01 \pm 0.90) \text{‰}$ (mean \pm 95 % confidence limit) for the YRD (Figure 4) and ($-$
366 $25.23 \pm 0.74) \text{‰}$ for Nanjing (Figure 5).

367 Figure 6 shows the monthly isotopic ratio calculated with the Miller-Tans method for the
368 whole observation period. The reader is reminded here that the results obtained for the
369 daytime and the nighttime period represent sources in the YRD and in Nanjing, respectively.
370 During the two and a half years of observation, the monthly δ_s for the YRD was lower in the

371 winter $[(-24.37 \pm 0.71) \text{‰}]$ and higher in the summer $(-23.42 \pm 1.79 \text{‰})$. The seasonal
372 difference for Nanjing was smaller than for the YRD $[(-24.87 \pm 0.51) \text{‰}]$ in the winter
373 (December to February) and $-24.80 \pm 1.79 \text{‰}$ in the summer months (June to August)]. The
374 sources in the YRD had slightly higher δ_s than those in in Nanjing. The mean δ_s value of the
375 whole observational period was $(-24.37 \pm 0.61) \text{‰}$ and $(-24.58 \pm 0.44) \text{‰}$ for the YRD and
376 Nanjing, respectively. The monthly δ_s for the YRD (Figure 6a) was highly correlated with the
377 monthly atmospheric $\delta^{13}\text{C}$ [Figure 2; $\delta_s = (2.29 \pm 0.78) \delta^{13}\text{C} + (-5.71 \pm 6.37)$, linear correlation
378 coefficient = 0.47, n = 30, p < 0.01]. The correlation between the monthly δ_s for Nanjing
379 (Figure 6b) and the monthly atmospheric $\delta^{13}\text{C}$ was weak [$\delta_s = (2.39 \pm 0.92) \delta^{13}\text{C} + (-3.71 \pm$
380 $8.07)$, linear correlation coefficient = 0.03, n = 30, p = 0.87]. These correlation patterns
381 suggest that atmospheric $\delta^{13}\text{C}$ was influenced more by surface sources at the regional scale
382 than at the local (city) scale.

383

384 **3.3 Inventory data for anthropogenic sources**

385 The emission strength of anthropogenic sources and their $^{13}\text{C}/^{12}\text{C}$ ratios were calculated with
386 the inventory method and the data found in the literature, as described in section 2.3. In the
387 YRD, coal combustion was by far the largest source of anthropogenic CO_2 , contributing 70 %
388 of the overall “fossil-plus” emission (Table 2). Here the “fossil-plus” emission includes
389 contributions from all forms of fossil fuel combustion and from non-cement industrial
390 processes. The second and third largest source were ammonia synthesis and pig iron
391 manufacturing, with fractional contributions of about 9 %. The “fossil-plus” source

392 contribution to the total anthropogenic emission was 91 %, with the remaining 9 %
393 contributed by cement production (Table 2).

394 In the Nanjing municipality, the fractional contribution of coal to the “fossil-plus” total
395 was 52 %, lower than that for the YRD, and the other three major sources were ammonia
396 synthesis (16 %), pig iron (13 %), and gasoline (11 %). The fractional contribution of fuel-
397 plus sources to the total anthropogenic emission was 96.4 % and the fractional contribution of
398 cement production was 3.6 % (Table 2). The isotopic ratio of the “fossil-plus” sources was
399 0.35 ‰ lower for Nanjing than for the YRD.

400 The overall effective isotopic ratio of the anthropogenic sources weighted by the source
401 contributions was also lower for Nanjing than for the YRD (Table 3). The difference was
402 1.76 ‰ and was a result of lower fractional contributions in Nanjing of coal combustion and
403 cement production, which have relatively high ^{13}C contents, and a higher fractional
404 contribution of natural gas, which is the fuel type with the lowest ^{13}C content.

405

406 **3.4. CO₂ fluxes in YRD and Nanjing**

407 Figure 7 shows the biological flux F_P and surface flux F_S calculated from the mass balance,
408 and the cement flux F_C and “fossil-plus” F_F . The F_P flux obtained with the isotopic
409 partitioning method for the YRD agreed with the seasonal phenology expected for plants in
410 this region. It was near zero or slightly negative in the summer and generally positive in the
411 winter, indicating uptake and release, respectively. The annual mean daytime biological flux
412 was $(0.03 \pm 0.64) \text{ mg m}^{-2} \text{ s}^{-1}$ in the YRD in the calendar year 2014. The net surface flux F_S
413 was $(0.17 \pm 2.02) \text{ mg m}^{-2} \text{ s}^{-1}$ in 2014. The standard deviations of these estimates are quite

414 large. If the extreme standard deviations of F_p ($5.16 \text{ mg m}^{-2} \text{ s}^{-1}$) and F_s ($22.00 \text{ mg m}^{-2} \text{ s}^{-1}$) in
415 March 2014 were excluded, the mean standard deviation of F_p would decrease to 0.23 mg m^{-2}
416 s^{-1} for and that of F_s to $0.20 \text{ mg m}^{-2} \text{ s}^{-1}$.

417 In Nanjing, the biological flux was positive throughout the year (Figure 8). This is
418 because the partitioning was done for the night hours when the natural ecosystems were a
419 source of CO_2 due to autotrophic and heterotrophic respiration. The annual mean nighttime
420 biological flux for the calendar year 2014 was $(0.06 \pm 0.26) \text{ mg m}^{-2} \text{ s}^{-1}$. The nighttime surface
421 flux was $(0.18 \pm 0.22) \text{ mg m}^{-2} \text{ s}^{-1}$ in 2014.

422

423 **4 Discussion**

424 **4.1 CO_2 mole fraction and $\delta^{13}\text{C}$ seasonality**

425 The atmospheric CO_2 mole fraction observed in Nanjing showed very small seasonal
426 variation (summer versus winter difference of $7.9 \mu\text{mol mol}^{-1}$, July versus January difference
427 of $15.6 \mu\text{mol mol}^{-1}$), in comparison with the data published for other cities. For example, in
428 Salt Lake City, USA, the CO_2 mole fraction in the summer is about $31 \mu\text{mol mol}^{-1}$ lower than
429 in the winter (Pataki et al., 2003). Several factors contributed to the weak seasonality in
430 Nanjing. The climate in the YRD is relatively mild. The governmental energy policy prohibits
431 winter heating in public buildings. Most residential buildings also lack space heating in the
432 winter. This is in contrast to energy use patterns in northern cities in China and elsewhere.
433 The weak seasonality of the observed mole fraction was also related to the low vegetation
434 cover in the YRD and in Nanjing. The forest cover ratio is about 35 % in Nanjing and in the
435 YRD, and the overall vegetation cover (forest plus other vegetation types) ratio in the major

436 cities in the YRD is lower than 45 % (CESY, 2013; CSY, 2013). For comparison, the
437 vegetation cover ratio is 56 % in Salt Lake City (Pataki et al. 2009) and 44 % in Chicago
438 (Rose et al. 2003). Dense vegetation is known to deplete atmospheric CO₂ in the summer
439 season via photosynthetic uptake, amplifying the CO₂ seasonal amplitude.

440 Our $\delta^{13}\text{C}$ seasonal amplitude (January versus July difference of 1.44 ‰) was 4 times the
441 amplitude observed or estimated at WLG (Figure 2) but agreed with those reported by most
442 urban studies. For comparison, the seasonal amplitude of $\delta^{13}\text{C}_a$ in Bangalore, India, was 0.89
443 to 1.32 ‰ (Guha and Ghosh 2015). Similar amplitudes have also been reported for Chicago
444 (January versus August difference of 1.25 ‰; Moore and Jacobson, 2015) and Beijing
445 (2.13 ‰; Pang et al. 2016). In Salt Lake City, the seasonal amplitude of $\delta^{13}\text{C}$ was
446 approximately 1.6 ‰ because of much more natural gas consumption for heating in the
447 winter than in the summer (Pataki et al. 2006).

448

449 **4.2 Influences of cement production on atmospheric $\delta^{13}\text{C}$**

450 The high summer $\delta^{13}\text{C}$ was one of the most unique characteristics at our site. The daytime
451 $\delta^{13}\text{C}$ reached -6.90 ‰ in July 2013 and -7.21 ‰ in August 2014, which were 1.28 ‰ and
452 0.95 ‰ higher than the WLG values. The highest monthly mean $\delta^{13}\text{C}$ occurred in July: -
453 7.44 ‰ in July 2013, -7.99 ‰ in July 2014 and -7.46 ‰ in July 2015. These values were
454 0.74 ‰, 0.16 ‰ and 0.77 ‰ higher than the WLG value reported for the same months.

455 The high July values observed at our site cannot be fully explained by CO₂ removal by
456 plant photosynthesis. Photosynthesis and respiration are the two processes that dominate the
457 ¹³C/¹²C seasonality in plant-dominated landscapes, leading to higher $\delta^{13}\text{C}$ values in the

458 summer and lower values in the winter. For example, in Park Falls, Wisconsin, USA, a site in
459 a heavily-forested landscape, $\delta^{13}\text{C}$ was -7.75‰ in August 2011 and -8.77‰ in February
460 2012 (Moore and Jacobson, 2015). For comparison, $\delta^{13}\text{C}$ was -8.24‰ and -8.38‰ at the
461 Mauna Loa Observatory and -8.02‰ and -8.66‰ at WLG in these two months, respectively.
462 In other words, the photosynthetic effect raised the August $\delta^{13}\text{C}$ by 0.5‰ above the
463 background value, a smaller enrichment than observed at our site. Because of the low
464 vegetation fraction, the summer photosynthetic CO_2 uptake in the YRD and in Nanjing
465 should be lower than at Park Falls. According to the CarbonTracker inversion analysis (Peters
466 et al. 2007), the net ecosystem production at the grid point where Park Falls is located is -
467 $0.201\text{ mg m}^{-2}\text{ s}^{-1}$ in July, 2014 but is only $-0.059\text{ mg m}^{-2}\text{ s}^{-1}$ at the grid point corresponding to
468 the YRD region. We would expect from the photosynthetic effect alone that the summertime
469 ^{13}C enrichment at our site to be smaller, not greater than that observed at Park Falls.

470 Furthermore, in a human-dominated landscape, the plant photosynthetic enhancement of
471 ^{13}C is offset by the CO_2 from fossil fuel combustion which has lower $^{13}\text{C}/^{12}\text{C}$ ratios than the
472 atmosphere. In Chicago, the monthly mean $\delta^{13}\text{C}$ peaked in August at -8.29‰ during the
473 calendar year 2011, which is 0.05‰ lower than the WLG value for the same month.
474 Similarly, in Beijing, the monthly mean $\delta^{13}\text{C}$ peaked at -9.49‰ in August 2014, which is
475 1.23‰ lower than the WLG value for the same month.

476 We suggest that cement production was the contributing factor responsible for the high
477 $\delta^{13}\text{C}$ values in the summer. The evidence supporting this interpretation is provided by data in
478 Table 3 and Figure 7. The delta value of anthropogenic CO_2 in the YRD would be $(-26.36 \pm$
479 $0.42)\text{‰}$ without cement production and increased to $(-23.95 \pm 0.41)\text{‰}$ after inclusion of the

480 cement source (Table 3). This value is much higher than those reported for other urban lands,
481 such as -30.7 ‰ for Los Angeles, USA (Newman et al. 2008) and about -31 ‰ for Salt Lake
482 City, USA (Bush et al. 2007). The overall surface source $^{13}\text{C}/^{12}\text{C}$ ratio derived from
483 atmospheric measurements (Figure 6; -24.37 ‰ and -24.58 ‰ for the YRD and Nanjing,
484 respectively) was also more enriched than those obtained from atmospheric measurements in
485 other cities, such as (-28.1 ± 0.8) ‰ for Chicago in August and September (Moore and
486 Jacobson, 2015), -32.4 ‰ to -27.4 ‰ for Salt Lake City in the growing season (Pataki et al.
487 2003), -27.0 ‰ for Beijing in the winter heating season (Pang et al. 2016), and -29.3 ‰ for
488 Los Angeles, USA (Newman et al. 2008).

489 The influence of cement production on atmospheric $\delta^{13}\text{C}$ has also been suggested for at
490 least two other urban sites. In Bangalore, India, $\delta^{13}\text{C}$ is 0.05 ‰ higher than that observed at
491 an island station in the Indian Ocean, and cement production in southern India is offered as a
492 reason to explain the enrichment of urban $\delta^{13}\text{C}$ (Guha and Ghosh 2015). The other urban site
493 is Beijing, China, where the $\delta^{13}\text{C}$ measurement may have been influenced by cement factories
494 outside the city (Ren et al. 2015, Pang et al. 2016).

495

496 **4.3 Net surface and biological fluxes in the YRD**

497 As a human-dominated landscape, the YRD was a net source of CO_2 on the monthly scale
498 even in the growing season (F_s , Figure 7). The seasonal trends of the net surface flux F_s and
499 the biological flux F_p were highly correlated with each other ($R^2 = 0.88$ after exclusion of
500 three extreme outliers) because the anthropogenic source strengths were almost constant. The
501 mean F_s between March 2013 and February 2015 was (0.19 ± 1.16) $\text{mg m}^{-2} \text{s}^{-1}$, which

502 consisted of (0.15 ± 0.02) $\text{mg m}^{-2} \text{s}^{-1}$ from fossil combustion and industrial processes, $(0.02 \pm$
503 $0.002)$ $\text{mg m}^{-2} \text{s}^{-1}$ from cement production and (0.05 ± 1.31) $\text{mg m}^{-2} \text{s}^{-1}$ from biological
504 activities. The total anthropogenic CO_2 flux was (0.17 ± 0.02) $\text{mg m}^{-2} \text{s}^{-1}$ in the YRD, a 70 %
505 increase from the value of $0.10 \text{ mg m}^{-2} \text{s}^{-1}$ reported for 2009 (Shen et al. 2014). From 2009 to
506 2012, the GDP increased by 56 % according to the National Statistic Yearbook.

507 For comparison, we extracted the flux data from the CarbonTracker database for the 6
508 by 6 pixels that cover the YRD region. The results show that the mean daytime (11:00 to
509 17:00 local time) biological flux is slightly negative at $-0.01 \text{ mg m}^{-2} \text{s}^{-1}$ for 2014 (Peter et al.
510 2007). Our estimate of F_P for 2014 was (0.03 ± 0.64) $\text{mg m}^{-2} \text{s}^{-1}$. As pointed out earlier, the F_P
511 value for March 2014 was highly uncertain [(0.21 ± 5.16) $\text{mg m}^{-2} \text{s}^{-1}$]; If we replace this value
512 by the mean value of February and April 2014, the 2014 mean F_P would be reduced to $(0.02 \pm$
513 $0.22)$ $\text{mg m}^{-2} \text{s}^{-1}$.

514 A source of uncertainty in our flux partitioning analysis is related to human breath (Affek
515 and Eiler 2006). Using the method of Prairie and Duarte (2007), we estimated that human
516 respiration flux was 0.006 and $0.013 \text{ mg m}^{-2} \text{s}^{-1}$, or 3.7 % and 11.65 % of anthropogenic
517 emission in the YRD and in Nanjing, respectively. The food diet in the region is
518 predominantly C3 grains. By including this additional source in Equations 3 and 4 and by
519 assuming that the isotopic ratio of digestion is the same as δ_P shown in Table 3, F_S and F_P
520 would increase by 0.008 and $0.001 \text{ mg m}^{-2} \text{s}^{-1}$ in the YRD and by $0.018 \text{ mg m}^{-2} \text{s}^{-1}$ and 0.005
521 $\text{mg m}^{-2} \text{s}^{-1}$ in Nanjing, respectively.

522

523 **4.4 Comparison of the Miller-Tans and the Keeling methods**

524 By applying the Miller-Tans method to daytime and nighttime observations separately, we
525 obtained the effective source ratios that are consistent with the inventory analysis for the
526 YRD and for the Nanjing Municipality. The daytime measurement (Figure 6a, solid circles)
527 revealed that the $^{13}\text{C}/^{12}\text{C}$ ratio of the all sources (anthropogenic and biological) was on
528 average 0.21 ‰ higher than that obtained with the nighttime measurement (Figure 6b, solid
529 circles), although the difference is not statistically significant ($p = 0.38$). For comparison, the
530 overall δ_s of the anthropogenic sources in the YRD was also higher than that in Nanjing, the
531 difference being 2.01 ‰ (Table 3). The interpretation that the daytime observations capture
532 the influence of surface sources in the YRD region is supported by a trajectory analysis and
533 by an analysis of the atmospheric methane to CO_2 emissions ratio observed at the same site
534 (Shen et al. 2014). We note that the atmospheric measurements gave a smaller difference
535 between the YRD and Nanjing than that obtained by the inventory data, likely because of
536 different biological contributions between the two spatial scales.

537 One open question with regard to the modified Miller-Tans method is what constitutes
538 the true background air for the YRD. In this study, the background was assumed to be the
539 tropospheric air above the YRD. The background delta value (δ_b) backed out from the
540 intercepts shown in Figures 4 and 5 is -7.6 ‰, which is higher than expected, suggesting that
541 the true background concentration C_b may be higher than the tropospheric value. One
542 noteworthy feature about Equation 3 is that its slope parameter is not sensitive to C_b , but its
543 intercept parameter is. By increasing C_b by $15 \mu\text{mol mol}^{-1}$, the slope of the regression in
544 Figure 5 would remain unchanged, but the δ_b backed out from the new intercept value would
545 become more reasonable (-8.23 ‰). In Newman et al. (2016), the background air was

546 measured at a coastal location upwind of the Los Angeles airshed. It is recommended that a
547 similar strategy should be used in future experiments, where simultaneous measurement is
548 made at the coast of East China Sea and only data collected in easterly winds are selected for
549 the Miller-Tans analysis.

550 We also calculated the $^{13}\text{C}/^{12}\text{C}$ ratio of the surface sources with the Keeling plot method.
551 Using the daytime data, the Keeling result was lower and more variable than that inferred
552 from the Miller-Tans method using the daytime data (Figure 6a). The two methods differed
553 by an average of -1.51 ‰ (Supplementary Table S2).

554 In comparison, the Keeling plot method showed reasonably good performance when
555 applied to the nighttime observations. This is because surface inversion conditions effectively
556 prevented mixing of the free atmospheric air with the surface air, so that the single-source
557 assumption implicit in the Keeling plot method could be satisfied. When we applied Keeling
558 plot method at monthly intervals to the nighttime data, the resulting δ_s showed very similar
559 month-to-month variations with the value obtained with application of the Miller-Tans
560 method to the nighttime observations (Figure 6b). The two method differed by an average of
561 1.21 ‰ (Supplementary Table S2).

562 When the δ_s derived from the Keeling plot method was used for flux-partitioning, the
563 results were much more erratic than shown in Figures 7 and 8 (Supplementary Figures S4 and
564 S5). The uncertainty ranges of the monthly F_P and F_S were two to three times larger. The
565 biological flux F_P for the YRD was out of range for 4 months, and did not display an obvious
566 seasonal pattern (Supplementary Figure S4). These results support our choice of the modified

567 Miller-Tans method as the preferred approach for inferring the overall $^{13}\text{C}/^{12}\text{C}$ ratio of the
568 surface sources in this study.

569

570 **5. Conclusions**

571 We showed that the temporal changes of $\delta^{13}\text{C}$ followed the seasonal patterns of
572 anthropogenic and biologic CO_2 emissions, with lower values in the winter than in the
573 summer. An unusual feature that has not been seen in other urban environments is that the
574 $\delta^{13}\text{C}$ exceeded that of the background atmosphere in some of the summer months. The
575 highest monthly $\delta^{13}\text{C}$ was -7.44‰ observed in July 2013, which was 0.74‰ greater than the
576 WLG value for the same month. Evidence points to cement production as the key reason for
577 why the atmospheric $\delta^{13}\text{C}$ was higher than at the background site. In contrast to the isotope
578 ratio, the CO_2 mole fraction displayed very weak seasonality (July to January difference 15.6
579 $\mu\text{mol mol}^{-1}$).

580 We hypothesized that the Miller-Tans method applied to the daytime and nighttime
581 observations should yield the effective $^{13}\text{C}/^{12}\text{C}$ ratio of surface sources at the regional (YRD)
582 and the local (Nanjing) scale, respectively. According to the results of the modified Miller-
583 Tans method, the effective source $^{13}\text{C}/^{12}\text{C}$ ratio in the YRD was -24.37‰ , which was 0.21‰
584 higher than that in the Nanjing Municipality. These results were consistent with inventory
585 estimates of anthropogenic source ratios at these two spatial scales.

586 By combining inventory data on anthropogenic carbon sources and the atmospheric
587 measurement of CO_2 mole fraction and $^{13}\text{C}/^{12}\text{C}$ ratio in an isotopic partitioning framework,
588 we inferred that natural ecosystems in the YRD were a negligibly small source of

589 atmospheric CO₂, with an average flux of (0.02 ± 0.22) mg m⁻² s⁻¹ for 2014. For comparison,
590 the CarbonTracker inverse analysis reveals a small annual mean daytime biological flux (-
591 0.01 mg m⁻² s⁻¹) for this region for 2014.

592

593 **Data availability:**

594 The atmospheric data are available upon request and from the Yale-NUIST Center website
595 <http://yncenter.sites.yale.edu>.

596

597 **Acknowledgments:**

598 This research was supported by the National Natural Science Foundation of China (Grant
599 41475141, 41505005), the U. S. National Science Foundation (Grant 1520684), the Ministry
600 of Education of China (Grant PCSIRT), and the Priority Academic Program Development of
601 Jiangsu Higher Education Institutions (Grant PAPD). The first author also acknowledged a
602 visiting scholarship from China Scholarship Council and a Graduate Student Innovation
603 Grant from Jiangsu Provincial Government (Grant KYLX_0848). We thank the handling
604 editor Dr. Jan Kaiser and four anonymous reviewers whose constructive comments have
605 greatly improved this paper.

606

References

607

Affek, H. P., Eiler, J. M. (2006). Abundance of mass 47-CO₂ in urban air, car exhaust, and human breath. *Geochimica et Cosmochimica Acta* **70**(1): 1-12.

608

609

610

Akbari H, Menon S, Rosenfeld A. Global cooling: increasing world-wide urban albedos to offset CO₂. *Climatic Change*, 2009, **94**(3-4): 275-286.

611

612

613

An, H (2012) Ammonia synthesis: current status and future outlook (in Chinese), *Coal Chemistry of Western China*, **2**: 4-13.

614

615

616

Andres, R. J., Marland, G., Boden, T., Bischof, S. (1994). Carbon dioxide emissions from fossil fuel consumption and cement manufacture, 1751-1991; and an estimate of their isotopic composition and latitudinal distribution, Oak Ridge National Lab., TN (United States);

617

618

619

620

Bai, Y., (2011) A Comparative Study on Turbulent Fluxes Exchange over Nanjing Urban and Suburban in Summer (in Chinese), Master's Thesis, Nanjing University of Information Science & Technology.

621

622

623

Ballantyne, A. P., Miller, J. B., Baker, I. T., Tans, P. P., White, J. W. C. (2011). Novel applications of carbon isotopes in atmospheric CO₂: what can atmospheric measurements teach us about processes in the biosphere? *Biogeosciences*, 8(10), 3093-3106.

624

625

626

Ballantyne, A. P., Miller, J. B., Tans, P. P. (2010). Apparent seasonal cycle in isotopic discrimination of carbon in the atmosphere and biosphere due to vapor pressure deficit. *Global Biogeochemical Cycles*, 24(3), 1-16.

627

628

629

Bowling, D. R., S P Burns, T. J. Conway, R. K. Monson, and J. W. C. White (2005) Extensive observations of CO₂ carbon isotope content in and above a high-elevation subalpine forest, *Global Biogeochemical Cycles*, **19**: GB3023.

630

631

632

Bi, J., Zhang, R., Wang, H., Liu, M., Wu, Y. (2011). The benchmarks of carbon emissions and policy implications for China's cities: Case of Nanjing. *Energy Policy* **39**(9): 4785-4794.

633

634

635

Bowling, D. R., Sargent, S. D., Tanner, B. D., and Ehleringer, J. R. (2003). Tunable diode laser absorption spectroscopy for stable isotope studies of ecosystem-atmosphere CO₂ exchange, *Agric. Forest Meteorol.*, **118**: 1-19.

636

637

638

Bush, S. E., Pataki, D.E., Ehleringer, J.R. (2007). Sources of variation in $\delta^{13}\text{C}$ of fossil fuel emissions in Salt Lake City, USA. *Applied Geochemistry* **22**(4): 715-723.

639

640

641

642

643

644

645

646

647 CESY (2013). China Energy Statistical Yearbook 2013: China Statistical Publishing House,
648 Beijing. (in Chinese) Also available at: <[http://www.stats.gov.cn/tjsj/ndsj/
649 2013/indexch.htm](http://www.stats.gov.cn/tjsj/ndsj/2013/indexch.htm)>.
650

651 Clark-Thorne, S. T., C. J. Yapp (2003). Stable carbon isotope constraints on mixing and mass
652 balance of CO₂ in an urban atmosphere: Dallas metropolitan area, Texas, USA. *Applied
653 Geochemistry* **18**(1): 75-95.
654

655 Coutts, A. M., Beringer, J., Tapper, N.J. (2007). Characteristics influencing the variability of
656 urban CO₂ fluxes in Melbourne, Australia. *Atmospheric Environment* **41**(1): 51-62.
657

658 China Cement: <http://hy.ccement.com/map/>, last access: 6 July 2016 (in Chinese).
659

660 CSY (2013). China Statistical Yearbook. National Bureau of Statistics of China. (in Chinese)
661 Also available at: <<http://www.stats.gov.cn/tjsj/ndsj/2013/indexch.htm>>
662

663 Duan Y. (1995) Study of characteristics of coal isotope composition in China. *Coal Geology &
664 Exploration* **23**(1) 29-33.
665

666 Ehleringer, J.R., Bowling, D.R., Flanagan, L.B., Fessenden, J., Helliker, B., Martinelli, L.A.,
667 Ometto, J.P. (2002). Stable isotopes and carbon cycle processes in forests and grasslands.
668 *Plant biology* **4**(2): 181-189.
669

670 Farquhar, G., J. Lloyd (1993). Carbon and oxygen isotope effects in the exchange of carbon
671 dioxide between terrestrial plants and the atmosphere. *Stable isotopes and plant carbon-water
672 relations* **40**: 47-70.
673

674 Fessenden, J. E., J. R. Ehleringer (2002). Age-related variations in $\delta^{13}\text{C}$ of ecosystem
675 respiration across a coniferous forest chronosequence in the Pacific Northwest. *Tree
676 Physiology* **22**(2-3): 159-167.
677

678 Friedman, L., A. P. Irsa (1967). Variations in isotopic composition of carbon in urban
679 atmospheric carbon dioxide. *Science* **158**(3798): 263-264.
680

681 Gorski G, Strong C, Good S P, Bares, R., Ehleringer, J. R., Bowen, G. J. (2015). Vapor
682 hydrogen and oxygen isotopes reflect water of combustion in the urban atmosphere.
683 *Proceedings of the National Academy of Sciences*, **112**(11): 3247-3252.
684

685 Griffis, T. J., Lee, X., Baker, J.M., Sargent, S.D., King, J.Y. (2005). Feasibility of quantifying
686 ecosystem-atmosphere C¹⁸O¹⁶O exchange using laser spectroscopy and the flux-gradient
687 method. *Agricultural and Forest Meteorology*, **135**(1-4): 44-60.
688

689 Griffis, T J. (2013). Tracing the flow of carbon dioxide and water vapor between the
690 biosphere and atmosphere: A review of optical isotope techniques and their application.
691 *Agricultural and Forest Meteorology*, **174**:85-109.
692

693 Guha, T., P. Ghosh (2010). Diurnal variation of atmospheric CO₂ concentration and delta C-
694 13 in an urban atmosphere during winter-role of the nocturnal boundary layer. *Journal of*
695 *Atmospheric Chemistry*, **65**(1): 1-12.
696

697 Guha, T. and P. Ghosh (2015). Diurnal and seasonal variation of mixing ratio and delta C-13
698 of air CO₂ observed at an urban station Bangalore, India. *Environmental Science and*
699 *Pollution Research*, **22**(3): 1877-1890.
700

701 ICLEI (International Council for Local Environmental Initiatives). (2008). Local government
702 operations protocol for the quantification and reporting of greenhouse gas emissions
703 inventories. [Available online at [http://www.arb.ca.gov/cc/protocols/localgov/archive/final](http://www.arb.ca.gov/cc/protocols/localgov/archive/final_lgo_protocol_2008-09-25.pdf)
704 [lgo protocol 2008-09-25.pdf.](http://www.arb.ca.gov/cc/protocols/localgov/archive/final_lgo_protocol_2008-09-25.pdf)]
705

706 Jasechko, S., Gibson, J. J., Edwards, T. W. (2014). Stable isotope mass balance of the
707 Laurentian Great Lakes. *Journal of Great Lakes Research*, **40**(2), 336-346.
708

709 Jasek, A., Zimnoch, M., Gorczyca, Z., Smula, E., Rozanski, K. (2014). Seasonal variability of
710 soil CO₂ flux and its carbon isotope composition in Krakow urban area, Southern Poland.
711 *Isotopes in Environmental and Health Studies*, **50**(2): 143-155.
712

713 Keeling, C. D. (1958). The concentration and isotopic abundances of atmospheric carbon
714 dioxide in rural areas. *Geochimica et Cosmochimica Acta*, **13**(4): 322-334.
715

716 Keeling, C. D. (1961). The concentration and isotopic abundances of carbon dioxide in rural
717 and marine air. *Geochimica et Cosmochimica Acta*, **24**(3): 277-298.
718

719 Koerner, B., J. Klopatek (2002). Anthropogenic and natural CO₂ emission sources in an arid
720 urban environment. *Environmental Pollution*, **116**: S45-S51.
721

722 Leavitt, S. W., Paul, E.A., Galadima, A., Nakayama, F.S., Danzer, S.R., Johnson, H., Kimball,
723 B.A. (1995). Carbon isotopes and carbon turnover in cotton and wheat FACE experiments.
724 *Plant and Soil* **187**(2): 147-155.
725

726 Lee, X., Sargent, S., Smith, R., & Tanner, B. (2005). In situ measurement of the water vapor
727 ¹⁸O/¹⁶O isotope ratio for atmospheric and ecological applications. *Journal of Atmospheric and*
728 *Oceanic Technology*, **22**(5), 555-565.
729

730 Lichtfouse, E., Lichtfouse, M., Jaffrezic, A. (2003). delta C-13 values of grasses as a novel
731 indicator of pollution by fossil-fuel-derived greenhouse gas CO₂ in urban areas.
732 *Environmental Science & Technology*, **37**(1): 87-89.

733
734 Liu, H., Feng, J., Järvi, L., Vesala, T. (2012). Four-year (2006–2009) eddy covariance
735 measurements of CO₂ flux over an urban area in Beijing. *Atmospheric Chemistry and*
736 *Physics*, **12**(17): 7881-7892.

737
738 Lloyd, J., Kruijt, B., Hollinger, D.Y., Grace, J., Francey, R.J., Wong, S., Kelliher, F.M.,
739 Miranda, A.C., Farquhar, G.D., Gash, J.H.C. (1996). Vegetation effects on the isotopic
740 composition of atmospheric CO₂ at local and regional scales: theoretical aspects and a
741 comparison between rain forest in Amazonia and a boreal forest in Siberia. *Functional Plant*
742 *Biology*, **23**(3): 371-399.

743
744 Lloyd, J., Francey, R.J., Mollicone, D., Raupach, M.R, Sogachev, A., Arneth, A., Byers, J.N.,
745 Kelliher, F.M., Rebmann, C., Valentini, R. (2001). Vertical profiles, boundary layer budgets,
746 and regional flux estimates for CO₂ and its ¹³C/¹²C ratio and for water vapor above a
747 forest/bog mosaic in central Siberia. *Global Biogeochemical Cycles*, **15**(2): 267-284.

748
749 McDonald, B.C., McBride, Z. C., Martin, E. W., Harley, R. A. (2014). High-resolution
750 mapping of motor vehicle carbon dioxide emissions. *Journal of Geophysical Research:*
751 *Atmospheres*, **119**(9): 5283-5298.

752
753 McManus, J. B., Zahniser, M.S., Nelson, D.D., Williams, L.R., Kolb, C.E. (2002). Infrared
754 laser spectrometer with balanced absorption for measurement of isotopic ratios of carbon
755 gases. *Spectrochimica Acta Part A: Molecular and Biomolecular Spectroscopy*, **58**(11): 2465-
756 2479.

757
758 Miller, J. B., P. P. Tans (2003). Calculating isotopic fractionation from atmospheric
759 measurements at various scales, *Tellus B*, **55**(2): 207-214.

760
761 Miller, J.B., Tans, P.P., White, J.W.C., Conway, T.J., Vaughn, B.W. (2003). The atmospheric
762 signal of terrestrial carbon isotopic discrimination and its implication for partitioning carbon
763 fluxes, *Tellus B*, **55**(2): 197-206.

764
765 Moore J., Jacobson A.D. (2015). Seasonally varying contributions to urban CO₂ in the
766 Chicago, Illinois, USA region: Insights from a high-resolution CO₂ concentration and d¹³C
767 record. *Elementa: Science of the Anthropocene*, **3**: 000052.

768
769 Mu, H., Li, H., Zhang, M., Li, M. (2013). Analysis of China's carbon dioxide flow for 2008.
770 *Energy Policy* **54**: 320-326.

771
772 Newman, S., Xu, X., Gurney, K.R., Hsu, Y.K., Li, K.F., Jiang, X., Keeling, R., Feng, S.,
773 O'Keefe, D., Patarasuk, R. and Wong, K.W. (2016). Toward consistency between trends in
774 bottom-up CO₂ emissions and top-down atmospheric measurements in the Los Angeles
775 megacity. *Atmospheric Chemistry and Physics*, **16**(6):3843-3863.

776

777
778 Newman, S., Xu, X., Affek, H.P., Stolper, E., Epstein, S. (2008). Changes in mixing ratio and
779 isotopic composition of CO₂ in urban air from the Los Angeles basin, California, between
780 1972 and 2003, *Journal of Geophysical Research*, **113**(D23): 1-15.
781
782 NSY (2013). Nanjing Statistical Yearbook. Nanjing Municipal Bureau Statistics. (in Chinese)
783 Also available at: < <http://www.njtz.gov.cn/2004/2013/renmin/index.htm>>
784
785 Ometto, J. P., Flanagan, L.B., Martinelli, L.A., Moreira, M.Z., Higuchi, N., Ehleringer, J.R.
786 (2002). Carbon isotope discrimination in forest and pasture ecosystems of the Amazon Basin,
787 Brazil, *Global Biogeochemical Cycles*, **16**(4):1-10.
788
789 Ometto, J.P., Ehleringer, J.R., Domingues, T.F., Berry, J.A., Ishida, F.Y., Mazzi, E., Higuchi,
790 N., Flanagan, L.B., Nardoto, G.B., Martinelli, L.A. (2006). The stable carbon and nitrogen
791 isotopic composition of vegetation in tropical forests of the Amazon Basin, Brazil,
792 *Biogeochemistry*, **79**(1-2): 251-274.
793
794 Pan, J. (2007) Theoretical and Process Studies of the Abatement of Fuel Gas Emissions
795 during Iron Ore Sintering (in Chinese), PhD Dissertation, Southcentral Univeristy of China.
796
797 Pang, J., Wen, X., Sun, X. (2016). Mixing ratio and carbon isotopic composition investigation
798 of atmospheric CO₂ in Beijing, China. *Sci Total Environ*, **539**: 322-330.
799
800 Pataki, D. E., Bowling, D.R., Ehleringer, J.R. (2003). Seasonal cycle of carbon dioxide and
801 its isotopic composition in an urban atmosphere: Anthropogenic and biogenic effects. *Journal*
802 *of Geophysical Research-Atmospheres*, **108**(D23): 1-8.
803
804 Pataki, D. E., Bowling, D.R., Ehleringer, J.R., Zobitz, J.M. (2006). High resolution
805 atmospheric monitoring of urban carbon dioxide sources. *Geophysical Research Letters*,
806 **33**(3): 1-5.
807
808 Pataki, D. E., Ehleringer, J.R., Flanagan, L.B., Yakir, D., Bowling, D.R., Still, C.J.,
809 Buchmann, N., Kaplan, J.O., Berry, J.A. (2003). The application and interpretation of Keeling
810 plots in terrestrial carbon cycle research. *Global Biogeochemical Cycles*, **17**(1): 1-14
811
812 Pataki, D. E., Lai, C., Keeling, C.D., Ehleringer, J.R. (2007). Insights from stable isotopes on
813 the role of terrestrial ecosystems in the global carbon cycle. *Terrestrial Ecosystems in a*
814 *Changing World*, Springer: 37-44.
815
816 Pataki, D.E., Emmi, P.C., Forster, C.B., Mills, J.I., Pardyjak, E.R., Peterson, T.R.,
817 Thompson, J.D., Dudley-Murphy, E., An integrated approach to improving fossil fuel
818 emissions scenarios with urban ecosystem studies. *Ecological Complexity*, 2009, **6**(1): 1-14.
819

820 Peters, W., Jacobson, A.R., Sweeney, C., Andrews, A.E., Conway, T.J., Masarie, K., Miller,
821 J.B., Bruhwiler, L.M., Petron, G., Hirsch, A.I., Worthy, D.E., van der Werf, G.R., Randerson,
822 J.T., Wennberg, P.O., Krol, M.C., Tans, P.P. (2007) An atmospheric perspective on North
823 American carbon dioxide exchange: CarbonTracker, Proceedings of the National Academy of
824 Sciences, **104**(48): 18925-18930.

825
826 Prairie, Yves T., Duarte, C. M. (2007). Direct and indirect metabolic CO₂ release by
827 humanity. Biogeosciences, **4**(2): 215-217.

828
829 Rella, C. (2011). Accurate stable carbon isotope ratio measurements with rapidly varying
830 carbon dioxide concentrations using the Picarro δ¹³C G2101-i gas analyzer, Picarro White
831 Paper. Picarro Inc.

832
833 Ren, L., Wang, W., Wang, J., Liu, R. (2015). Analysis of energy consumption and carbon
834 emission during the urbanization of Shandong Province, China. Journal of Cleaner
835 Production, **103**: 534-541.

836
837 Röckmann¹ T, S Eyer, C. van der Veen¹, ME Poppa, B Tuzson, G Monteil¹, S Houweling,
838 Eliza Harris, D Brunner, H Fischer, G Zazzeri, D Lowry, EG Nisbet, WA Brand, JM Necki, L
839 Emmenegger, and J Mohn (2016). In situ observations of the isotopic composition of
840 methane at the Cabauw tall tower site. Atmos. Chem. Phys., **16**: 10469–10487.

841
842 Rose L S, Akbari H, Taha H. Characterizing the fabric of the urban environment: a case study
843 of Greater Houston, Texas. Lawrence Berkeley National Laboratory, 2003.

844
845 Satterthwaite D. Cities' contribution to global warming: notes on the allocation of greenhouse
846 gas emissions. Environment and Urbanization, 2008, **20**(2): 539–549.

847
848 Shen, S., Yang, D., Xiao, W., Liu, S., Lee, X. (2014). Constraining anthropogenic CH₄
849 emissions in Nanjing and the Yangtze River Delta, China, using atmospheric CO₂ and CH₄
850 mixing ratios, Advances in Atmospheric Sciences, **31**(6): 1343-1352.

851
852 Song, T., Wang Y. (2012). Carbon dioxide fluxes from an urban area in Beijing. Atmospheric
853 Research, **106**: 139-149.

854
855 Sturm, P., Leuenberger, M., Valentino, F. L., Lehmann, B. and Ihly B. (2006). Measurements
856 of CO₂, its stable isotopes, O₂/N₂, and ²²²Rn at Bern, Switzerland. Atmos. Chem. Phys., **6**:
857 1991–2004.

858
859 Sun, B., Dilcher, D.L., Beerling, D.J., Zhang, C., Yan, D., Kowalski, E. (2003). Variation in
860 Ginkgo biloba L. leaf characters across a climatic gradient in China. Proceedings of the
861 National Academy of Sciences, **100**(12): 7141-7146.

862

863 Takahashi, H. A., Konohira, E., Hiyama, T., Minami, M., Nakamura, T., Yoshida, N. (2002).
864 Diurnal variation of CO₂ concentration, Delta C-14 and delta C-13 in an urban forest:
865 estimate of the anthropogenic and biogenic CO₂ contributions, *Tellus B*, **54**(2): 97-109.
866

867 Tans, P. (1981). ¹³C/¹²C of industrial CO₂. In *SCOPE 16: Carbon Cycle Modelling* (B.Bolin,
868 ed.), John Wiley and Sons, Chichester, England, 127-129.
869

870 Thoning, K. W., Tans, P.P., Komhyr, W.D. (1989). Atmospheric carbon dioxide at Mauna Loa
871 Observatory: 2. Analysis of the NOAA GMCC data, 1974–1985. *Journal of Geophysical*
872 *Research*, **94**(D6): 8549-8565.
873

874 Sanam Noreen Vardag, S. N., S. Hammer, I. Levin (2016) Evaluation of 4 years of continuous
875 ¹³C(CO₂) data using a moving Keeling plot method, *Biogeosciences*, *Biogeosciences*, **13**:
876 4237–4251.
877

878 Wada, R., Nakayama, T., Matsumi, Y., Hiyama, T., Inoue, G., Shibata, T. (2011). Observation
879 of carbon and oxygen isotopic compositions of CO₂ at an urban site in Nagoya using Mid-IR
880 laser absorption spectroscopy. *Atmospheric Environment*, **45**(5): 1168-1174.
881

882 Wang, D. (2013) *Method and Empirical Research of Urban Greenhouse Gas Measurement* (in
883 Chinese), Master's Thesis, Tianjin University.
884

885 Wang, W. , D. E. Pataki (2012). Drivers of spatial variability in urban plant and soil isotopic
886 composition in the Los Angeles basin. *Plant and Soil*, **350**(1-2): 323-338.
887

888 Wen, X. F., Meng, Y., Zhang, X., Sun, X., Lee, X. (2013). Evaluating calibration strategies
889 for isotope ratio infrared spectroscopy for atmospheric ¹³CO₂/¹²CO₂ measurement.
890 *Atmospheric Measurement Techniques*, **6**(1): 795-823.
891

892 Wehr, R., and S. R. Saleska (2017) The long-solved problem of the best-fit straight line:
893 application to isotopic mixing lines, *Biogeosciences*, **14**: 17-29.
894

895 Widory, D. (2006). Combustibles, fuels and their combustion products: A view through
896 carbon isotopes. *Combustion Theory and Modelling*, **10**(5): 831-841.
897

898 Widory, D., M. Javoy (2003). The carbon isotope composition of atmospheric CO₂ in Paris.
899 *Earth and Planetary Science Letters*, **215**(1-2): 289-298.
900

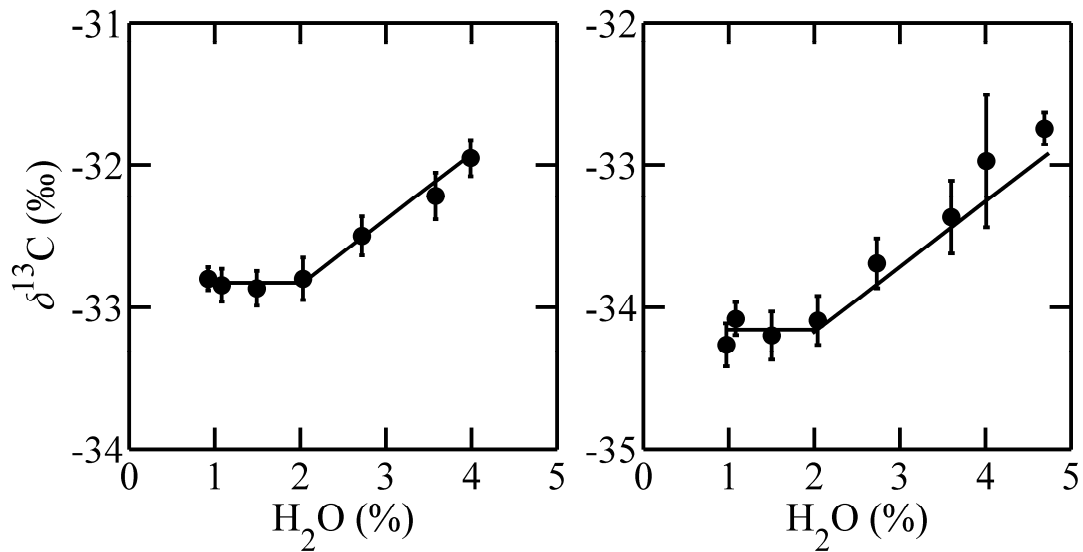
901 Yakir, D., L. da SL Sternberg (2000). The use of stable isotopes to study ecosystem gas
902 exchange. *Oecologia*, **123**(3): 297-311.
903

904 Yang, H.M., Wang, H.Z. , Wu, Y.B. (2011). Observation and characteristics analysis of traffic
905 flow in Nanjing. (in Chinese), *Environmental Science and Technology*, **24**(2): 98-101.
906

907 Zimnoch, M., Florkowski, T., Necki, J. M., Neubert, R. E. (2004). Diurnal variability of $\delta^{13}\text{C}$
908 and $\delta^{18}\text{O}$ of atmospheric CO_2 in the urban atmosphere of Kraków, Poland. *Isotopes in*
909 *Environmental and Health Studies*, **40**(2), 129-143.
910
911 Zobitz, J. M., Burns, S.P., Reichstein, M., Bowling, D.R. (2008). Partitioning net ecosystem
912 carbon exchange and the carbon isotopic disequilibrium in a subalpine forest. *Global Change*
913 *Biology*, **14**(8): 1785-1800.
914
915 Zondervan, A., H. A. Meijer (1996). Isotopic characterisation of CO_2 sources during regional
916 pollution events using isotopic and radiocarbon analysis. *Tellus B*, **48**(4): 601-612.
917
918 Zhou, L., Conway, T.J., White, J.W., Mukai, H., Zhang, X., Wen, Y., Li, J. and MacClune, K.,
919 (2005). Long-term record of atmospheric CO_2 and stable isotopic ratios at Waliguan
920 Observatory: Background features and possible drivers, 1991–2002. *Global Biogeochemical*
921 *Cycles*, **19**(3): GB3021.
922

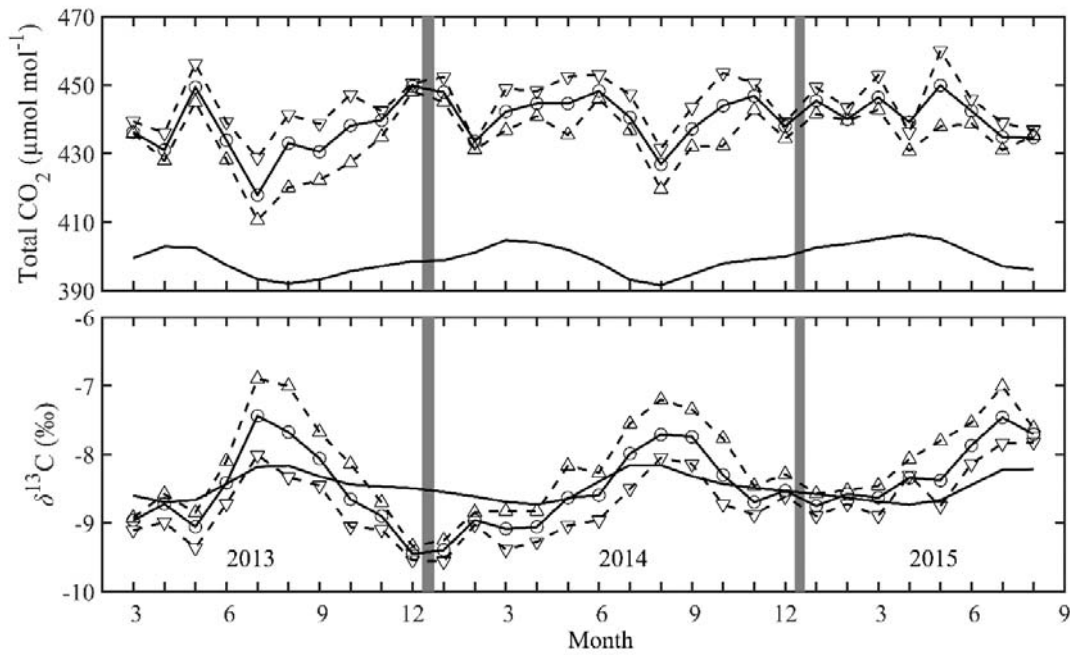
923 **Figure 1.** Dependence of the observed $\delta^{13}\text{C}$ on the H_2O mole fraction. The lines represent
924 Equation 2. Error bars are \pm one standard deviation of 1-min averages. The data in the left
925 panel was obtained on October 1, 2014 using a $439 \mu\text{mol mol}^{-1}$ standard gas and the true $\delta^{13}\text{C}$
926 value of -32.8 ‰ , and that in the right panel on June 10, 2015 using a $488 \mu\text{mol mol}^{-1}$
927 standard gas and the true $\delta^{13}\text{C}$ value of -34.1 ‰ .

928



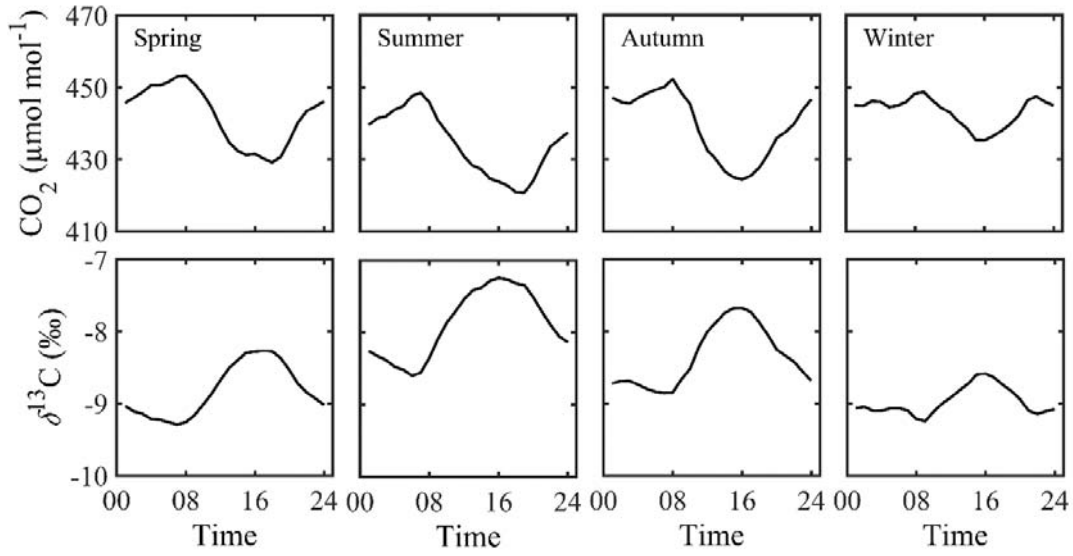
929

930 **Figure 2.** Monthly total CO₂ mole fraction (upper panel) and δ¹³C (lower panel): Solid lines
 931 with circles: whole-day means; dashed lines with up triangles: daytime (10:00-16:00) means;
 932 dashed line with down triangles: nighttime (22:00-6:00) means; smooth solid lines, monthly
 933 means observed at WLG.



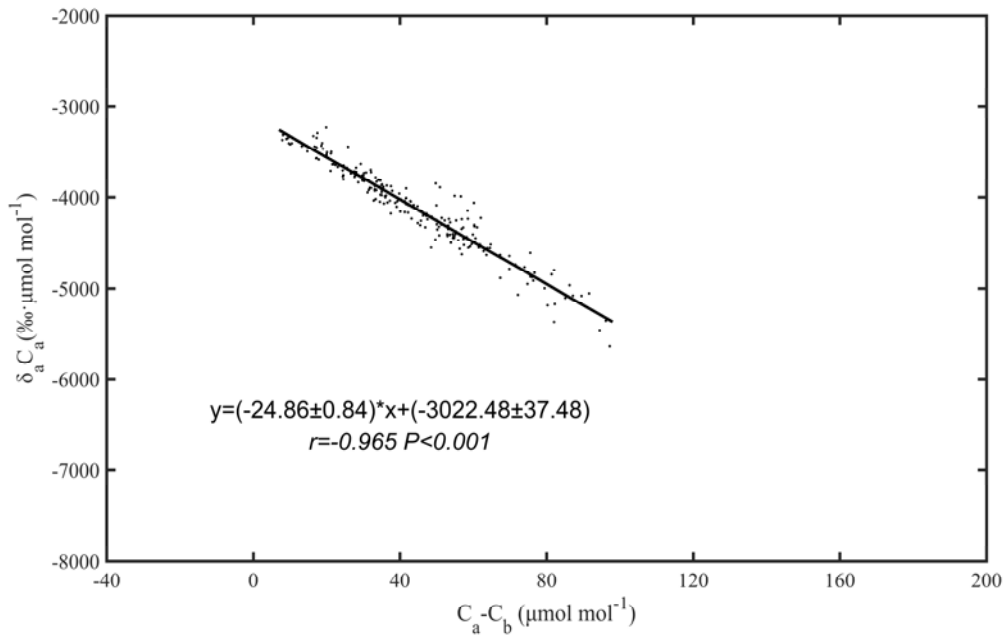
934
 935
 936

937 **Figure 3.** Mean diel variation of the CO₂ mole fraction (upper panels) and the $\delta^{13}\text{C}$ value
938 (bottom panels) between March, 2013 and August, 2015.



939
940

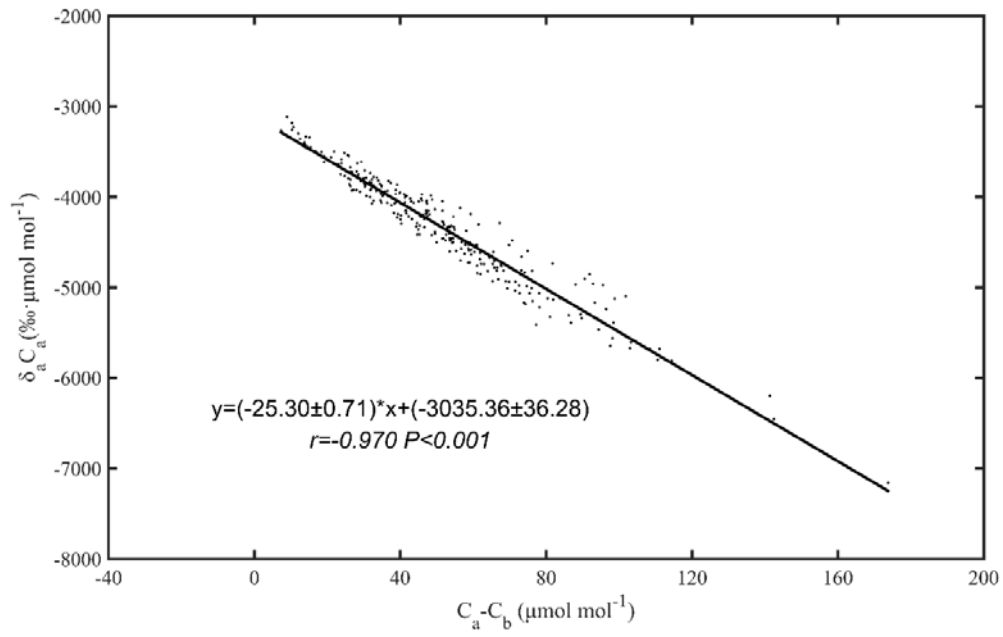
941 **Figure 4.** Application of the Miller-Tans method to the daytime (10:00-16:00) data obtained
942 in January 2014. Each data point is one hourly mean. The solid line is the least squares
943 regression according to Equation 3. Errors bounds on the regression coefficients are 95 %
944 confidence intervals.



945

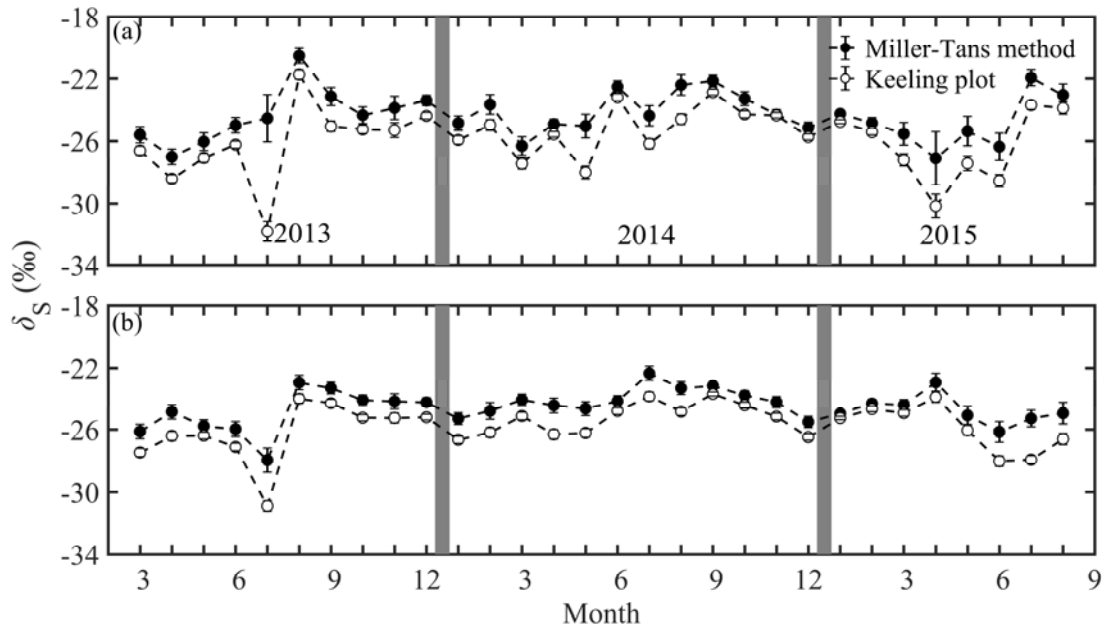
946

Figure 5. Same as Figure 4 but for nighttime (22:00-6:00) data obtained in January 2014.



947

948 **Figure 6.** Time series of monthly $^{13}\text{C}/^{12}\text{C}$ ratio of surface sources in the YRD (a) and in
949 Nanjing (b), obtained from daytime and nighttime measurement, respectively. The error bars
950 are \pm one standard deviation of the regression coefficient.



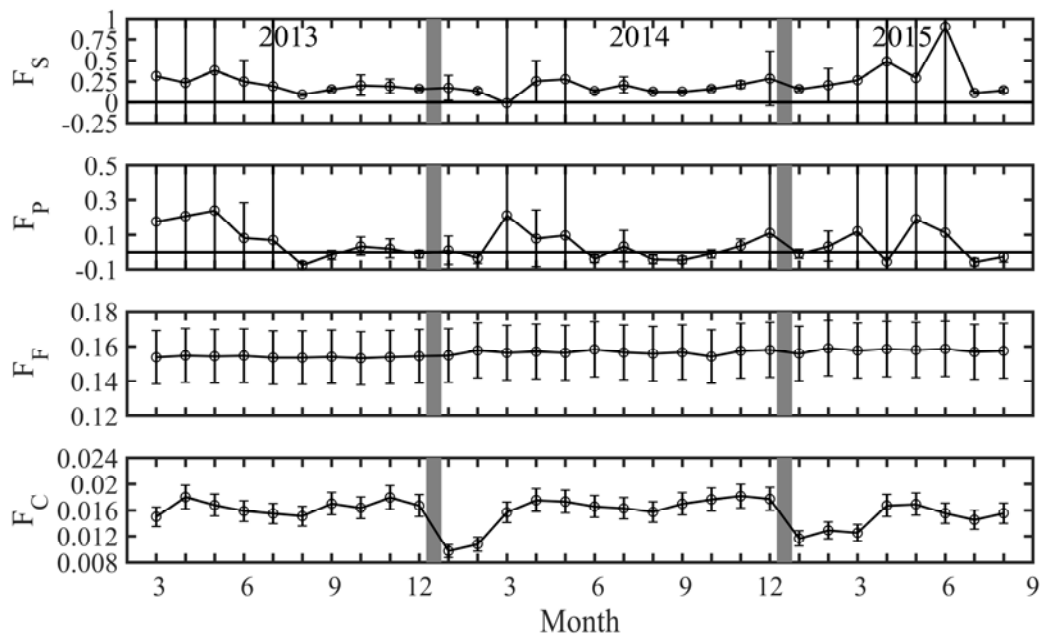
951

952

953

954

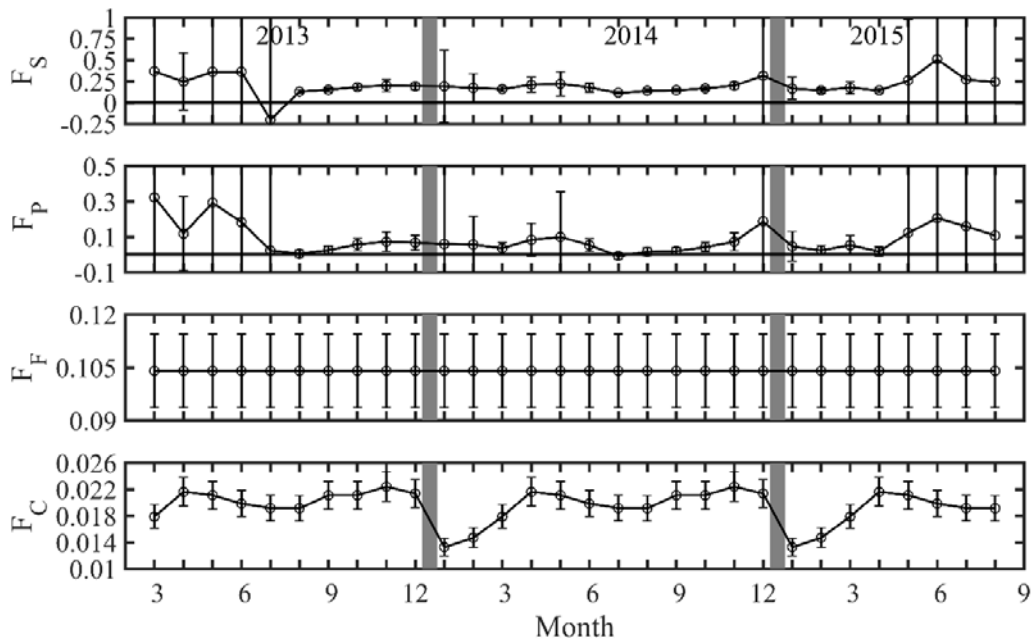
955 **Figure 7.** Time series of monthly net surface CO₂ flux (F_S), biological CO₂ flux (F_P),
 956 anthropogenic CO₂ flux excluding cement emission (F_F) and cement CO₂ flux (F_C) in the
 957 YRD. All the CO₂ mass fluxes are in $\text{mg m}^{-2} \text{s}^{-1}$. The flux terms F_F and F_C are assumed to have
 958 a 10 % uncertainty typical of fossil fuel consumption data. The partitioning results (F_P and
 959 F_S) are based on the source $^{13}\text{C}/^{12}\text{C}$ ratio derived from daytime atmospheric measurements.



960
 961

962 **Figure 8.** Time series of monthly net surface CO₂ flux (F_S), biological CO₂ flux (F_P),
 963 anthropogenic CO₂ flux excluding cement emission (F_F) and cement CO₂ flux (F_C) in
 964 Nanjing. All the CO₂ mass fluxes are in $\text{mg m}^{-2} \text{s}^{-1}$. The flux terms F_F and F_C are assumed to
 965 have a 10 % uncertainty typical of fossil fuel consumption data. The partitioning results (F_P
 966 and F_S) are based on the source $^{13}\text{C}/^{12}\text{C}$ ratio derived from nighttime atmospheric
 967 measurements.

968



969

970 **Table 1** Standard gases used for instrument calibration. The mean and standard deviation of
971 the CO₂ mole fraction and $\delta^{13}\text{C}$ were based on 6 and 5 repeated measurements, respectively.

ID	CO ₂ ($\mu\text{mol mol}^{-1}$)	$\delta^{13}\text{C}$ (‰)	Period
1 Low	381.89 ± 0.99	-29.75 ± 0.27	Mar, 2013 - Aug, 2014
1 High	502.35 ± 0.28	-30.01 ± 0.18	Mar, 2013 - Aug, 2014
2 Low	380.92 ± 0.95	-29.75 ± 0.27	Sep, 2014 - Aug, 2015
2 High	501.05 ± 0.33	-30.01 ± 0.18	Sep, 2014 - Aug, 2015

972

973 **Table 2** Percentage of “fossil-plus” sources and their $\delta^{13}\text{C}$ values for the YRD and Nanjing.

974 The uncertainty in the total “fossil-plus” source is a weighted mean of the individual

975 uncertainties.

Sources	Percentage (%)		$\delta^{13}\text{C}$ (‰)		References
	YRD	Nanjing	YRD	Nanjing	
Coal	70.0	52.3	-25.46 ± 0.39	-25.46 ± 0.39	Duan, 1995, Widory 2003
Gasoline	2.1	11.4	-28.69 ± 0.50	-28.69 ± 0.50	Widory and Javoy 2003
Diesel	3.2	1.6	-28.93 ± 0.26	-28.93 ± 0.26	Widory 2006
Fuel oil	2.1	0.3	-29.32 ± 0.15	-29.32 ± 0.15	Widory and Javoy 2003
Natural gas	2.7	5.0	-39.06 ± 1.07	-39.06 ± 1.07	Widory 2003
LPG	0.7	0.2	-31.70 ± 0.40	-31.70 ± 0.40	Widory 2006
Pig iron	8.7	12.7	-24.90 ± 0.40	-24.90 ± 0.40	Pan 2007
Crude steel	1.5	0.7	-25.28 ± 0.40	-25.28 ± 0.40	Wang 2013
Ammonia synthesis	9.0	15.9	-28.18 ± 0.55	-28.18 ± 0.55	An 2012
Total	100	100	-26.36 ± 0.42	-26.97 ± 0.46	

976

977 **Table 3.** Inventory data for the isotopic composition of surface CO₂ sources and their
 978 percentage of contribution in the YRD and in Nanjing. Here the “fossil-plus” category
 979 includes all non-cement anthropogenic emissions listed in Table 2. The cement isotopic ratio
 980 is based on Andres et al. (1994). The uncertain range in the biological isotope ratio is based
 981 on Vardag et al. (2016).

Sources	YRD		Nanjing	
	$\delta^{13}\text{C}$ (‰)	Percentage (%)	$\delta^{13}\text{C}$ (‰)	Percentage (%)
“Fossil-plus”	-26.36 ± 0.42	91.0	-26.97 ± 0.46	96.4
Cement	0 ± 0.30	9.0	0 ± 0.30	3.6
Anthropogenic	-23.99 ± 0.41	100	-26.00 ± 0.45	100
Biological	-28.20 ± 1.00	—	-28.20 ± 1.00	—

982